Weak values in nonideal spin measurements: An exact treatment beyond the asymptotic regime

A. K. Pan and A. Matzkin

Laboratoire de Physique Théorique et Modélisation, CNRS Unité 8089, Université de Cergy-Pontoise, F-95302 Cergy-Pontoise Cedex, France

(Received 28 September 2011; published 24 February 2012)

We consider weak measurements (WMs) of a spin observable in quantum mechanics beyond the usual asymptotic regime. This is done by obtaining the exact time-dependent wave functions of the measuring apparatus for general nonideal measurements. Ideal strong measurements and the usual WM regime are obtained as the two extreme limiting cases of our exact treatment. We show that in the intermediate regime nonideal measurements lead to "semiweak" eccentric values that differ from the usual weak values. We further show that even in the WM regime the exact treatment leads to a meter behavior that can be markedly distinct from the one predicted by the usual WM formalism. We give several illustrations and discuss an application to the distinction of different realizations of the same density matrix.

DOI: 10.1103/PhysRevA.85.022122 PACS number(s): 03.65.Ta

I. INTRODUCTION

In recent times the issue of "weak measurement" (WM) in quantum mechanics has gained significant and wide interest in realizing apparently counterintuitive quantum effects. This path-breaking idea was originally proposed by Aharonov, Albert, and Vaidman (AAV) [1], who introduced a measurement scenario in quantum mechanics so that the empirically measured value (coined the "weak value") of an observable can be seemingly weird in that it yields results going beyond the eigenvalue spectrum of the measured observable. Since then, this idea has been enriched by a number of theoretical works [2–7] and experimental works [8–16]. This novel technique of obtaining a strange property of an observable has several implications, for example, providing insights into conceptual quantum paradoxes [3,4,17,18], identifying a tiny spin Hall effect [11], detecting very small transverse beam deflections [13], and measuring average quantum trajectories for photons [19].

It is well known that a standard quantum mechanical measurement requires a *strong* coupling in order to produce an *ideal* one-to-one correspondence between the measured system and the device state (for this reason, standard measurements are often termed to be *strong* or *ideal*). In contrast, the WM scheme, as the name suggests, assumes a very weak coupling (so that the system state is kept grossly undisturbed) and interfering device states (so that the coherence in the device remains intact). To observe an effect of this weak perturbation in the device pointer's state, it is necessary to suitably select a particular subensemble, which is technically termed "postselection." Given the initial state (known as the "preselected" state in AAV's terminology), any "weak value of an observable can be observed if the postselection is appropriately chosen. Weak values have another unusual property in that they can be complex. If the weak coupling approximation is made in the position coordinate, such as in a Stern-Gerlach (SG) setup, the real and imaginary parts of the complex weak value correspond to the momentum and position mean values of the postselected pointer state, respectively [6]. In this case, if the weak value is real, the effect can be observed in the momentum-space distribution of the pointer state; i.e., the peak of the momentum distribution is shifted by an amount proportional to the weak value, possibly several times the corresponding eigenvalue of the observable in question.

In the original AAV treatment, the WM scenario is obtained as an approximate limiting case for weak couplings and nearly overlapping device states, whereas strong projective measurements pertain to the opposite limiting case. However, between these two limiting cases there is a continuous range of situations encompassing different regimes that have been scarcely investigated. Recently, however, a few works [20–23] have studied the issue of WM beyond the usual approximations made in the AAV formalism. The specificity of our work is that we analyze the general case of nonideal measurements (followed by postselection) by starting from the *exact* solutions of the Schrödinger equations coupling the system and the measuring device. The standard WM regime then appears for weak couplings and nearly overlapping meter states. But the other "nonideal" measurement situations also display potentially interesting effects. We show, in particular, not only that in these regimes eccentric outcomes can be obtained, but also that the resulting "semiweak" or "generalized weak" values can be tuned at will, allowing the device's pointer to be shifted more than the weak value. We also show that it is possible to observe dichotomic outcomes of the pointer, as in the case of strong measurements, but with eccentric shifts, including in situations in which standard weak values cannot be defined. We further show that even in the standard WM regime, some effects neglected in the AAV treatment can lead to exact weak values markedly different from the usual WM ones. All these features are analyzed in a simple system that is analytically tractable: a spin-1/2 particle passing through a series of SG setups.

The paper is organized as follows. In Sec. II we briefly recapitulate the essence of the standard WM. In Sec. III we introduce a particle with spin 1/2 passing through a series of SG setups. The spatial wave packet is considered to be the probe that measures the particle's spin state. Rigorously solving the coupled solutions of the system allows us to define naturally the nonideal situation: the two limiting cases of strong and WMs are explicitly given; the peculiar features visible in the intermediate regime—the semiweak and the generalized weak values—are described. Our findings are illustrated in Sec. IV, and an application to a quantum

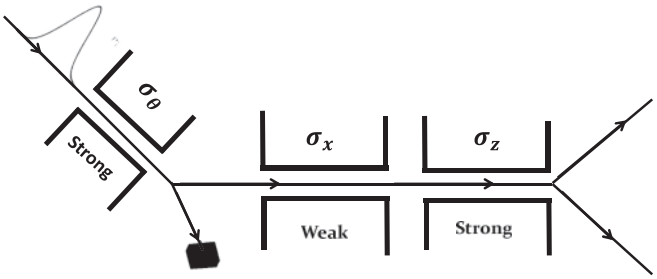

FIG. 1. A series of Stern-Gerlach (SG) setups for implementing weak measurements of the spin operator $\hat{\sigma}_x$. The three SG setups account, respectively, for the state preparation, the weak measurement, and the postselection.

information task is also considered. Our conclusions are given in Sec. V.

II. STANDARD WEAK MEASUREMENT SCENARIO

The entire process of the AAV WM procedure [1,3] consists of three steps: state preparation (usually termed preselection); a strong projective measurement for selecting a specific subensemble known as postselection; and in between the pre- and the postselection, a weak interaction, which is introduced so that the system state remains virtually unaffected by this intermediate interaction (see Fig. 1). AAV demonstrated the entire process in terms of a series of three SG setups. Let a beam of spin-1/2 neutral particles, say, neutrons, pass through the SG setups. The first SG is used to prepare the spin preselected state labeled $|\chi_{\rm in}\rangle$. The total initial wave function after the first SG setup is $\Psi_{\rm in} = \psi_0(x)|\chi_{\rm in}\rangle$. The spatial part $\psi_0(x)$ is taken to be a Gaussian wave packet peaked at the entry point ($x = 0$) of the second SG at $t = 0$:

$$\psi_0(x) = \frac{1}{(2\pi\delta^2)^{1/4}} \exp\left[-\frac{x^2}{4\delta^2}\right]. \tag{1}$$

For simplicity, the spatial part is written as being one-dimensional: the spatial wave functions along the y and z directions are trivial in that they are not affected by the SG interaction given below. The initial momentum-space wave function $\phi_0(p_x)$ corresponding to Eq. (1) is

$$\phi_0(p_x) = \left(\frac{2\delta^2}{\pi\hbar^2}\right)^{1/4} \exp\left(-\frac{\delta^2 p_x^2}{\hbar^2}\right). \tag{2}$$

Neutrons having the state $\Psi_{\rm in} = \psi_0(x)|\chi_{\rm in}\rangle$ then pass through the second SG setup, which is used for measuring a spin observable, say, $\widehat{\sigma}_x$. The interaction Hamiltonian is given by $H = f(t)\mu\widehat{\sigma}.\mathbf{B}$, where $\mathbf{B} = (bx,0,0)$ and μ is the magnetic moment of neutron. $f(t)$ is a smooth function of t vanishing outside the interval $0 < t < \tau$ and obeying $\int_0^\tau f(t)dt = \tau$, where τ is the transit time during which the neutrons interact with the magnetic field. The total state after the interaction can then be written as

$$\Psi' = e^{-\frac{i\mu b\tau x\hat{\sigma}_x}{\hbar}} \psi_0(x)|\chi_{\rm in}\rangle. \tag{3}$$

The spatial part of the wave function can be considered in the context of the SG setup to describe the state of the measurement device: in an SG, the spin state is inferred from the wave packet's deviation, which leads the particle to be found in the upper or lower planes when a strong measurement is performed.

Here, instead, the magnetic field and transit time are taken to be very small, so that the system state remains essentially unaltered by the interaction. Then the exponential in Eq. (3) can be expanded to first order. This is done in the original AAV treatment by performing, after the weak interaction, a strong projective measurement using the third SG setup. This "postselects" the neutrons in a definite final spin state $|\chi_f\rangle$. The postselection allows us to write the device state as

$$\begin{aligned}\psi_f(x) &= \langle\chi_f|e^{-\frac{i\mu b\tau x\sigma_x}{\hbar}}\psi_0(x)|\chi_{\rm in}\rangle \\ &= \langle\chi_f|1 - i\frac{\mu b\tau x\sigma_x}{\hbar} + o(2) - \ldots|\chi_{\rm in}\rangle\psi_0(x). \end{aligned}\tag{4}$$

Neglecting the higher order terms leads to

$$\psi_f(x) = \langle\chi_f|\chi_{\rm in}\rangle\left[1 - \frac{i\mu b\tau x}{\hbar}\frac{\langle\chi_f|\sigma_x|\chi_{\rm in}\rangle}{\langle\chi_f|\chi_{\rm in}\rangle}\right]\psi_0(x), \tag{5}$$

which can be written as

$$\psi_f(x) = \langle\chi_f|\chi_{\rm in}\rangle e^{-i\frac{\mu b\tau x}{\hbar}(\sigma_x)_w}\psi_0(x), \tag{6}$$

where

$$(\sigma_x)_w = \frac{\langle\chi_f|\sigma_x|\chi_{\rm in}\rangle}{\langle\chi_f|\chi_{\rm in}\rangle} \tag{7}$$

is known as the weak value of the observable $\widehat{\sigma}_x$.

This weak value appears as a phase shift in the pointer state's configuration-space wave function that determines the position of the pointer in momentum space. Taking the Fourier transform of Eq. (6), the pointer state in momentum space can be written as

$$\phi_f(p_x) = \langle\chi_f|\chi_{\rm in}\rangle\left(\frac{2\delta^2}{\pi\hbar^2}\right)^{1/4}\exp\left[-\frac{\delta^2(p_x - p'_x(\sigma_x)_w)^2}{\hbar^2}\right], \tag{8}$$

where $p'_x = \mu b\tau$. The final momentum distribution can then be written as

$$|\phi_f(p_x)|^2 = |\langle\chi_f|\chi_{\rm in}\rangle|^2|\phi_0(p_x - p'_x(\sigma_x)_w)|^2, \tag{9}$$

where $|\langle\chi_f|\chi_{\rm in}\rangle|^2$ is the probability of successful postselection. Hence the final pointer position in momentum space is shifted by an amount $(\sigma_x)_w p'_x$, in contrast to the strong measurement case, where the final pointer positions are shifted by $\pm p'_x$, corresponding to the eigenvalues ± 1 of $\hat{\sigma}_x$.

From Eq. (7) it can be seen that $(\sigma_x)_w$ can be exceedingly large if the preselected and postselected states are nearly orthogonal. Rescaling the momentum to p_x/p'_x, we see that the pointer displays a broad distribution centered on $(\sigma_x)_w$ [or the real part of $(\sigma_x)_w$, if the latter is complex], hence possibly well beyond the ranges of the eigenvalues. For instance, for a specific preselected state, say, $|\chi_{\rm in}\rangle = |\uparrow_\theta\rangle \equiv \cos\frac{\theta}{2}|\uparrow_z\rangle + \sin\frac{\theta}{2}|\downarrow_z\rangle$, and postselected state, say, $|\chi_f\rangle = |\uparrow\rangle_z$, the weak value of $\hat{\sigma}_x$ is given by $(\sigma_x)_w = \tan\frac{\theta}{2}$. According to this formalism, $(\sigma_x)_w$ can become arbitrarily large as $\theta \to \pi$, but simultaneously the probability of this

postselection, $|\langle\chi_f|\chi_{\rm in}\rangle|^2 = |\langle\uparrow_z \mid \uparrow_\theta\rangle|^2 = \cos^2\frac{\theta}{2}$, becomes vanishingly small (we see below, from the exact treatment, that both of these properties are erroneous, as the limit $\theta \to \pi$ is well defined). The final momentum distribution (9) after postselection can be written as

$$|\phi_f(p_x)|^2 = \cos^2\frac{\theta}{2}\left(\frac{2\delta^2}{\pi\hbar^2}\right)^{1/2}\exp\left[-\frac{2\delta^2\left(p_x - p_x'\tan\frac{\theta}{2}\right)^2}{\hbar^2}\right]. \tag{10}$$

Note that in deriving the above relations, we neglected the higher order terms in Eq. (4), which is justified [2] if, for $n \geqslant 2$,

$$\left(\frac{\mu b\tau}{\hbar}\right)^n |x^n\langle\chi_f|(\hat{\sigma}_x)^n|\chi_{\rm in}\rangle| \ll |\langle\chi_f|\chi_{\rm in}\rangle|,$$
$$\left(\frac{\mu b\tau}{\hbar}\right)^n |x^n\langle\chi_f|(\hat{\sigma}_x)^n|\chi_{\rm in}\rangle| \ll \frac{\mu b\tau}{\hbar}|x\langle\chi_f|\hat{\sigma}_x|\chi_{\rm in}\rangle|.$$

Moreover, in order to resum Eq. (5) into Eq. (6), we need $\mu b\tau x(\sigma_x)_w/\hbar \ll 1$; finally, noting that x is effectively governed by the spread δ, we may write the condition for the derivation as

$$\delta\frac{\mu b\tau}{\hbar}(\sigma_x)_w \ll 1. \tag{11}$$

III. BEYOND THE STANDARD WEAK MEASUREMENT REGIME

A. General remarks

The usual WM scheme, presented in Sec. II, involves rough approximations, some of which can usually be controlled (coupling value, width of device states); others, like the loss of unitarity due to the asymptotic expansion, have consequences that are more delicate to tackle within definite situations. Moreover, there remains a continuous range of regimes for which the approximations made in the standard WM derivation do not hold, though the situation is still far from the ideal strong measurement limit. These intermediate nonideal regimes, which can be referred to as "semiweak" situations, are considered in the present section.

We first give the exact solution for a nonideal SG, that is, solving the coupled Schrodinger equations for a wave packet of a spin-1/2 particle without making any specific assumptions for the coupling strength and the device states. We then see how semiweak outcomes are obtained when a strong measurement is added after the neutron has emitted the nonideal SG. A crucial quantity that we introduce is the overlap I of the wave packets (recall that the wave packets here play the role of the device states), which quantifies the strength of a given measurement situation. We indeed see that $I \to 0$ yields the strong ideal measurement regime, while $I \to 1$ corresponds to the usual AAV WM scheme. For an arbitrary value of I the superposition of the device states results in a distribution yielding the semiweak values. The different types of behavior of the pointer that can be obtained (one or several semiweak values, eccentric semiweak values, or semiweak values falling between the eigenvalues, exact weak values that take into account details of the interaction Hamiltonian) are also discussed. The illustrations are deferred to Sec. IV.

B. Neutrons passing through a nonideal SG setup: Exact solutions

The setup is the same as the one discussed in Sec. II (see Fig. 1). We omit the state preparation procedure and consider the initial spin state as given. Let a beam of neutrons passing through the second SG setup be represented by the total wave function

$$\Psi(\mathbf{x},t=0) \equiv \psi_0(\mathbf{x})|\uparrow\rangle_\theta, \tag{12}$$

where $|\uparrow\rangle_\theta = \cos\frac{\theta}{2}|\uparrow_z\rangle + \sin\frac{\theta}{2}|\downarrow_z\rangle$ is the initial state of the system (i.e., the spin). The spatial wave function $\psi_0(\mathbf{x})$ corresponds to a Gaussian wave packet that is initially peaked at $\mathbf{x} = 0$ at $t = 0$, given by

$$\psi_0(\mathbf{x}) = \frac{1}{(2\pi\delta^2)^{3/4}}\exp\left(-\frac{\mathbf{x}^2}{4\delta^2} + i\frac{p_y y}{\hbar}\right), \tag{13}$$

where δ is the initial width of the wave packet. The wave packet moves along the $+y$ axis with the initial momentum p_y (see Fig. 1). The inhomogeneous magnetic field $\mathbf{B} = (bx,0,0)$[1] is directed along the x axis and confined between $y = 0$ and $y = d$. The interaction Hamiltonian is $H_i = \mu\widehat{\sigma}.\mathbf{B}$, where, as above, μ is the magnetic moment of the neutron. As the wave packet propagates through the SG magnet, in addition to the $+y$ axis motion, the particles gain momentum along the $\pm x$ axis due to the interaction of their spins with the field. The time-evolved total wave function at τ (transit time of the peak of the wave packet within the SG magnetic field region) after the interaction of spins with the SG magnetic field is given by

$$\Psi(\mathbf{x},\tau) = \exp\left(-\frac{iH_i\tau}{\hbar}\right)\Psi(\mathbf{x},t=0)$$
$$= \alpha\psi_{+x}(\mathbf{x},\tau)\otimes|\uparrow\rangle_x + \beta\psi_{-x}(\mathbf{x},\tau)\otimes|\downarrow\rangle_x, \tag{14}$$

where the device states $\psi_{+x}(\mathbf{x},\tau)$ and $\psi_{-x}(\mathbf{x},\tau)$ are the two components of the spinor $\psi = \binom{\psi_+}{\psi_-}$, which satisfies the Pauli equation and $\alpha = \frac{1}{\sqrt{2}}(\cos\frac{\theta}{2} + \sin\frac{\theta}{2})$ and $\beta = \frac{1}{\sqrt{2}}(\cos\frac{\theta}{2} - \sin\frac{\theta}{2})$. Note that Eq. (14) is an entangled state between the position and the spin degrees of freedom. The reduced density matrix of the system in the x-basis representation can be written as

$$\rho_s = \begin{pmatrix}\alpha^2 & \alpha\beta I\\ \alpha\beta I^* & \beta^2\end{pmatrix}, \tag{15}$$

where I is the overlap

$$I = \int_v \psi_{+x}^*(\mathbf{x},\tau)\psi_{-x}(\mathbf{x},\tau)d^3x, \tag{16}$$

which quantifies the weakness of the measurement. The inner product I is, in general, complex, but here in our case I is

[1]This form of magnetic field is unphysical, as it does not satisfy the Maxwell equation $\nabla.\mathbf{B} = 0$. We need at least another component to make it divergence free [24]. However on average the effect of these additional field components can be neglected under proper circumstances, resulting in this effective field usually found in textbooks and also employed in Refs. [1,2].

always real and positive. The value of I can range from 0 to 1, depending on the choices of the relevant parameters, such as the degree of the magnetic field (b), the width of the initial wave packet (δ), and the transit time through the field region within the SG setup (τ). We calculate the analytical expressions of $\psi_{+x}(\mathbf{x},\tau)$ and $\psi_{-x}(\mathbf{x},\tau)$ by solving the relevant Schroedinger equations.

The two-component Pauli equation for ψ_{+x} and ψ_{-x} can then be written

$$i\hbar\frac{\partial\psi_{+x}}{\partial t} = -\frac{\hbar^2}{2m}\nabla^2\psi_{+x} + \mu b x\psi_{+x}, \tag{17}$$

$$i\hbar\frac{\partial\psi_{-x}}{\partial t} = -\frac{\hbar^2}{2m}\nabla^2\psi_{-x} - \mu b x\psi_{-x}. \tag{18}$$

The solutions of the above two equations at $t=\tau$ upon exiting the SG are as follows (for a detailed derivation, see Ref. [24]):

$$\psi_{+x}(\mathbf{x};\tau) = \frac{1}{(2\pi\delta^2)^{\frac{3}{4}}}\exp\left[-\frac{z^2+\left(y-\frac{p_y\tau}{m}\right)^2+\left(x-\frac{p'_x\tau}{2m}\right)^2}{4\delta^2}\right] \times \exp\left[i\left\{-\Delta+\left(y-\frac{p_y\tau}{2m}\right)\frac{p_y}{\hbar}+\frac{p'_x x}{\hbar}\right\}\right], \tag{19}$$

$$\psi_{-x}(\mathbf{x};\tau) = \frac{1}{(2\pi\delta^2)^{\frac{3}{4}}}\exp\left[-\frac{z^2+\left(y-\frac{p_y\tau}{m}\right)^2+\left(x+\frac{p'_x\tau}{2m}\right)^2}{4\delta^2}\right] \times \exp\left[i\left\{-\Delta+\left(y-\frac{p_y\tau}{2m}\right)\frac{p_y}{\hbar}-\frac{p'_x x}{\hbar}\right\}\right], \tag{20}$$

where $\Delta = \frac{p'^2_x\tau}{6m\hbar}$, $p'_x = \mu b\tau$, and the spreading of the wave packet is neglected throughout the evolution.

Here $\psi_{+x}(\mathbf{x},\tau)$ and $\psi_{-x}(\mathbf{x},\tau)$, representing the spatial wave functions at τ, correspond to the spin states $|\uparrow\rangle_x$ and $|\downarrow\rangle_x$, respectively, with the average momenta $\langle\widehat{p}\rangle_\uparrow$ and $\langle\widehat{p}\rangle_\downarrow$, where $\langle\widehat{p}\rangle_{\uparrow\downarrow} = (\pm p'_x, p_y, 0)$. Within the magnetic field the neutrons gain the same magnitude of momentum $p'_x = \mu b\tau$ but the directions are such that the particles with eigenstates $|\uparrow\rangle_x$ and $|\downarrow\rangle_x$ get the drift along the $+x$ axis and $-x$ axis, respectively, while the y-axis momenta remain unchanged.

From these analytical expressions of $\psi_{+x}(\mathbf{x},\tau)$ and $\psi_{-x}(\mathbf{x},\tau)$ given by Eqs. (19) and (20), it is straightforward to compute the inner product I [Eq.(16)], given by

$$I = \exp\left(-\frac{\mu^2 b^2\tau^4}{8m^2\delta^2} - \frac{2\mu^2 b^2\tau^2\delta^2}{\hbar^2}\right), \tag{21}$$

which explicitly depends on the choices of the parameters b, δ, and τ.

Now, after emerging from this nonideal SG magnet, the neutrons represented by the entangled state given by Eq. (14) enter another SG setup, where a strong measurement is to be performed and the neutrons are postselected in a specific spin state.

C. Subsequent strong measurement: Postselection and final pointer state

For this purpose, we consider, immediately after the wave packet exits the WM SG, a subsequent strong measurement of the spin observable $\widehat{\sigma}_z$. Knowledge of the exact solutions allows us to treat the strong measurements and WMs on the same footing. The approximate magnetic field in this case is $\mathbf{B} = (0,0,b'z)$, and T is the time during which the interaction occurs. A strong measurement requires the magnetic field b' to be sufficiently strong that the spatial wave packets emerging from this SG setup are orthogonal; i.e., the relevant inner product, analog to Eq. (21), vanishes. If the neutrons having the position-spin entangled state given by Eq. (14) enter the final SG setup, then the time evolved state that exits from the setup can be written as

$$\begin{aligned}\Psi(\mathbf{x},\tau+T) = {}& \frac{\alpha}{\sqrt{2}}\psi_{+x+z}(\mathbf{x},\tau+T)|\uparrow\rangle_z \\ &+ \frac{\alpha}{\sqrt{2}}\psi_{+x-z}(\mathbf{x},\tau+T)|\downarrow\rangle_z \\ &+ \frac{\beta}{\sqrt{2}}\psi_{-x+z}(\mathbf{x},\tau+T)|\uparrow\rangle_z \\ &+ \frac{\beta}{\sqrt{2}}\psi_{-x-z}(\mathbf{x},\tau+T)|\downarrow\rangle_z.\end{aligned} \tag{22}$$

The inner products $\langle\psi_{+x+z}|\psi_{+x-z}\rangle$ and $\langle\psi_{-x+z}|\psi_{-x-z}\rangle$ at $t=\tau+T$ vanish for strong measurements. The states $\psi_{\pm x\pm z}(\mathbf{x},\tau+T)$ can be calculated using $\psi_{+x}(\mathbf{x},\tau)$ and $\psi_{-x}(\mathbf{x},\tau)$, given by Eqs. (19) and (20), respectively, as the initial position wave functions. Note here that since the nonhomogeneous magnetic field is only along the z axis, within this SG setup, the neutrons move freely along the two other directions. Hence the analytical forms of the states $\psi_{\pm x\pm z}(\mathbf{x},\tau+T)$, are given by

$$\psi_{+x\ \pm z}(\mathbf{x};\tau+T) = \frac{1}{(2\pi\delta^2)^{\frac{3}{4}}}\exp\left[-\frac{\left(z\mp\frac{p_z T}{m}\right)^2+\left(y-\frac{p_y(\tau+T)}{2m}\right)^2+\left(x-\frac{p'_x\tau}{2m}-\frac{p'_x T}{m}\right)^2}{4\delta^2}\right] \times \exp\left[i\left\{-\Delta-\Delta'\pm\frac{p'_z z}{\hbar}+\left(y-\frac{p_y(\tau+T)}{2m}\right)\frac{p_y}{\hbar}+\frac{p'_x}{\hbar}\left(x-\frac{p'_x T}{2m}\right)\right\}\right], \tag{23}$$

$$\psi_{-x\ \pm z}(\mathbf{x};\tau+T) = \frac{1}{(2\pi\delta^2)^{\frac{3}{4}}}\exp\left[-\frac{\left(z\mp\frac{p_z T}{m}\right)^2+\left(y-\frac{p_y(\tau+T)}{2m}\right)^2+\left(x+\frac{p'_x\tau}{2m}+\frac{p'_x T}{m}\right)^2}{4\delta^2}\right] \times \exp\left[i\left\{-\Delta-\Delta'\pm\frac{p'_z z}{\hbar}+\left(y-\frac{p_y(\tau+T)}{2m}\right)\frac{p_y}{\hbar}-\frac{p'_x}{\hbar}\left(x+\frac{p'_x T}{2m}\right)\right\}\right], \tag{24}$$

where $\Delta' = \frac{p_z'^2 T}{6m\hbar}$ and $p_z' = \mu b' T$

Assume that we postselect the neutrons having spin state $|\uparrow_z\rangle$; then the postselected position-space wave function is written using Eq. (22), given by

$$\Psi_{\text{post}}(\mathbf{x},\tau+T) = \frac{1}{\sqrt{2}}[\alpha\psi_{+x+z}(\mathbf{x},\tau+T) + \beta\psi_{-x+z}(\mathbf{x},\tau+T)]. \quad (25)$$

The states $\psi_{+x+z}(\mathbf{x},T+\tau)$ and $\psi_{-x+z}(\mathbf{x},T+\tau)$ are separable in x,y,z and can thus be written with obvious notation as $\psi_{\pm x+z}(\mathbf{x},T+\tau) \equiv \psi'_{\pm x}(x,T+\tau)\psi_y(y,T+\tau)\psi_{+z}(z,T+\tau)$. Equation (25) becomes

$$\Psi_{\text{post}}(\mathbf{x},\tau+T) = \frac{1}{\sqrt{2}}\,\psi_y(y,T+\tau)\psi_{+z}(z,T+\tau) \times [\alpha\psi'_{+x}(x,T+\tau) + \beta\psi'_{-x}(x,T+\tau)]. \quad (26)$$

We see that the y- and z-dependent parts of the total wave functions do not play any significant role in this context and are thus integrated out. The motion along the $\hat{x}$ axis within the final SG setup is free so we can neglect the T dependence of $\psi'_{\pm x}(x,T+\tau)$. Thus the final postselected pointer wave function, depending only on x, can be written as

$$\Psi'_{\text{post}}(x,\tau) = \frac{1}{\sqrt{2}}[\alpha\psi'_{+x}(x,\tau) + \beta\psi'_{-x}(x,\tau)], \quad (27)$$

where

$$\psi'_{\pm x}(x,\tau) = \frac{1}{(2\pi\delta^2)^{\frac{1}{4}}}\exp\left[-\frac{\left(x \mp \frac{p'_x\tau}{m}\right)^2}{4\delta^2} \pm i\frac{p'_x x}{\hbar}\right] \quad (28)$$

is obtained from Eqs. (23) and (24).

The corresponding momentum-space wave function is

$$\Phi_{\text{post}}(p_x,\tau) = \frac{1}{\sqrt{2}}[\alpha\phi_{+x}(p_x,\tau) + \beta\phi_{-x}(p_x,\tau)], \quad (29)$$

where $\phi_{\pm x}$ are obtained by taking the Fourier transform of Eqs. (28), yielding, with ϕ_0 given by Eq. (3),

$$\phi_{\pm}(p_x,\tau) = \phi_0(p_x \mp p'_x) \times \exp\left(-\frac{ip_x^2\tau}{2m\hbar} \pm \frac{ip_x p'_x\tau}{2m\hbar} - \frac{i\mu^2 b^2\tau^3}{6m\hbar}\right). \quad (30)$$

The momentum-space solution, (29), is general in that no restriction on the coupling constant or on the width of the probe states hase been introduced. We can now look at the device's momentum distribution in different regimes, which are characterized by the value of I.

D. Strong measurement limit: $I \approx 0$

Let us now assume that we tune the relevant parameters (b, δ, and τ) so that $I \to 0$. In this case the reduced density matrix given by Eq. (15) of the system becomes

$$\rho_s = \begin{pmatrix} \alpha^2 & 0 \\ 0 & \beta^2 \end{pmatrix}, \quad (31)$$

which is diagonal, implying the strong measurement limit in that there is a one-to-one correspondence between the pointer state ϕ'_{+x} (ϕ'_{-x}) and the spin state $|\uparrow\rangle_x$ ($|\downarrow\rangle_x$). Hence, in this case we expect two spatially separated peaks pointing at the eigenvalues of the spin observables $\widehat{\sigma}_x$. In Fig. 2(a) we depict the device momentum distribution given by Eq. (29), where we find the peaks at $\pm p'_x$.

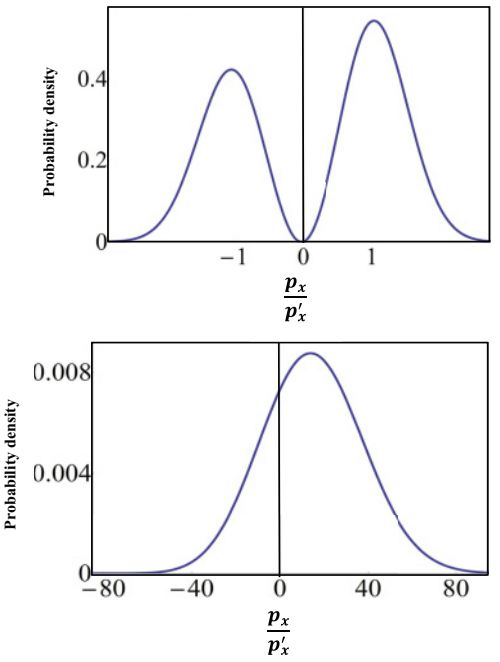

FIG. 2. (Color online) The momentum distribution $|\Phi_{\text{post}}(p_x,\tau)|^2$ [Eq. (29)] is plotted for (a) $I \approx 0$ (ideal projective measurement situation) and (b) $I \approx 1$ (weak measurement situation). Values of relevant parameters are $b = 100$ G/cm, $\tau = 1.4 \times 10^{-6}$ s, and $\delta = 1$ cm for (a) and $\delta = 1/50$ cm for (b). The weak value is $(\sigma_x)_w = 16.2$ for $\theta = 173.5^\circ$.

E. Standard weak measurement limit: $I \approx 1$

The WM limit is just the opposite limiting situation of strong measurement. From Eq. (21) we can see, for example, that for a fixed δ we can choose the other parameters, b and τ, such that $I \approx 1$ is obtained. The reduced density matrix of the system becomes

$$\rho_s \approx \frac{1}{2}\begin{pmatrix} \alpha^2 & \alpha\beta \\ \alpha\beta & \beta^2 \end{pmatrix};$$

i.e., the coherence in the system is considered to be mostly unaffected. There is no correspondence between the system and the device states. This leads to the usual WM scheme proposed by AAV. Indeed, let us start with the pointer position-space wave function given by Eq. (28), since the coupling is between the spin and the position variable. If the parameters b and τ are sufficiently small, the value of I could be close to unity for a fixed δ. In this case we can neglect the higher order terms of $b\tau$, keeping only first order term. We can then write the states $\psi'_{\pm x}(\mathbf{x};\tau)$ given by Eqs. (28) as

follows:

$$\psi'_{\pm x}(x;\tau) \approx \psi_0(x)(1 \pm i p'_x x/\hbar). \quad (32)$$

In this limit Eq.(27) becomes

$$\Psi'_{\rm post}(x,\tau) \approx \frac{\psi_0(x)}{\sqrt{2}}[\alpha(1 + i p'_x x/\hbar) + \beta(1 - i p'_x x/\hbar)]. \quad (33)$$

Setting the values of α, β, and $\psi_0(x)$ and simplifying, we get

$$\Psi'_{\rm post}(x,\tau) \approx \frac{\cos\frac{\theta}{2}}{(2\pi\delta^2)^{1/4}} \exp\left(-\frac{x^2}{4\delta^2} + i\frac{p'_x x \tan\frac{\theta}{2}}{\hbar}\right). \quad (34)$$

The Fourier transform of Eq. (34) gives the pointer wave function in momentum space, yielding the distribution

$$|\Phi_f(p_x)|^2 \approx \cos^2\frac{\theta}{2}\left(\frac{2\delta^2}{\pi\hbar^2}\right)^{1/2} \exp\left[-\frac{2\delta^2\left(p_x - p'_x\tan\frac{\theta}{2}\right)^2}{\hbar^2}\right], \quad (35)$$

which exactly matches Eq. (10) of the standard WM formulation.

F. Nonideal situations: Semiweak and exact weak values

When the overlap I lies in the intermediate range $0 < I < 1$, an imperfect coherence remains in the system state. After postselecting on a given final spin state, the pointer distribution is obtained from Eq. (27), therefore displaying an interference between the overlapping meter wave functions correlated with orthogonal spin states.

The pointer behavior depends on the details of the interference: by monitoring I, eccentric pointer shifts can be obtained in this intermediate range. We term these resulting shifts "semiweak" values. Depending on the resulting interference, which can be tuned by changing the values of the parameters (such as b, δ, and τ), the pointer distribution can display a single maximum, akin to the usual WM regime, with the additional feature that this maximum does not necessarily appear at the AAV weak value given by Eq. (7), but can be chosen by fine-tuning the parameters. Other behaviors of the pointer can be obtained, in particular, profiles with two maxima, similar to the two peaks that characterize the strong limit, but with the maxima shifted far from the eigenvalues.

Even in the usual $I \approx 1$ WM regime, pointer shifts can be obtained in cases in which the usual WM formalism does *not* predict any, such as in situations in which the pre- and postselected states are orthogonal. More importantly, when the oscillating terms in Eqs. (28) play a role (i.e., when the wavelength of the oscillation becomes of the order of magnitude of the distribution width), the meter distribution becomes significantly different from what is predicted by the usual WM formalism. The features produced by these "exact" weak values are illustrated below.

It is interesting to note that several recent works [20–23] have also attempted to go beyond the usual WM formalism in the weak regime. Wu and Li [21] took the asymptotic expansion to second order (one order beyond AAV's derivation) and showed that this was sufficient to treat the orthogonal pre- and postselected states case. These results were extended in Ref. [22], where it was shown that the asymptotic expansion can be resummed when weak values of projectors are considered. A different but equivalent approach [20,23] follows the early method of Sudarshan and collaborators [2], consisting in formally expanding the preselected state in terms of the eigenstate of the weakly measured operator. This allows us to recover the standard WM in the limit of weak couplings. The main difference between all these approaches and our present work lies not only in the method employed—we explicitly solve the full Schroedinger equation of the entire system (measured subsystem and pointer apparatus)—but also in the fact that, by doing so, we take into account the motion of the system and of the pointer, generated by the respective self-Hamiltonians. The strong, weak, or nonideal nature of the measurement is then seen to depend on characteristics of the full solution, not only on the coupling strength. For the WM of spin in an SG developed here, the different parameters that determine the nonideal character of the measurement were encapsulated in the quantity I.

IV. ILLUSTRATIONS AND APPLICATIONS

A. Semiweak value distributions

We give here an illustration of the properties of the meter state distributions in the nonideal regime giving rise to the semiweak values examined in Sec. III. For definiteness the examples given correspond to the explicit formulas given above, involving the initial wave function, Eq. (1), with the initial spin in state $|\uparrow\rangle_\theta$, an intermediate WM or semiweak measurement of the system (spin) observable $\hat{\sigma}_x$, and a final postselection along $|\uparrow\rangle_z$.

1. Strong and weak limits

Consider first the strong and weak limits. A typical example is given in Fig. 2, where the device state distributions are plotted in configuration (x) space as well as in momentum (P) space (recall that the only nontrivial axis is the one along x, the WM axis). For the strong case the postselection along $|\uparrow\rangle_z$ is applied after a first strong measurement along $\hat{\sigma}_x$ that couples perfectly each wave packet (meter state) with the relevant spin state $|\uparrow\rangle_x$ or $|\downarrow\rangle_x$. In **x** space this yields a single broad structure at the eigenvalue of the $\hat{\sigma}_z$ measurement, whereas in **P** space two peaks are visible [see Fig. 2(a)], each corresponding to the direction of the momentum along the x axis: the strong measurement condition perfectly correlates this momentum with the spin state.

In the weak limit, a single peak is still visible in x space, but in **P** space the two interfering Gaussians overlap almost perfectly ($I \approx 1$). The result is itself (approximately [2]) a Gaussian, as predicted by the WM formalism, but with a maximum displaced at the weak value $p'_x \tan\frac{\theta}{2}$ [see Fig. 2(b)]. The meter therefore has a broad distribution centered at a value several times higher than the spin eigenvalue, with the single peak pointing here at $(\sigma_x)_w = 16.2$ for $\theta = 173.5^\circ$.

2. Semiweak values

We first illustrate in Fig. 3 the generic situation as I is varied from the ideal strong situation ($I \approx 0$) to the weak limit ($I \approx 1$). We see that the meter distribution goes smoothly from the strong type of behavior to the one that characterizes the weak

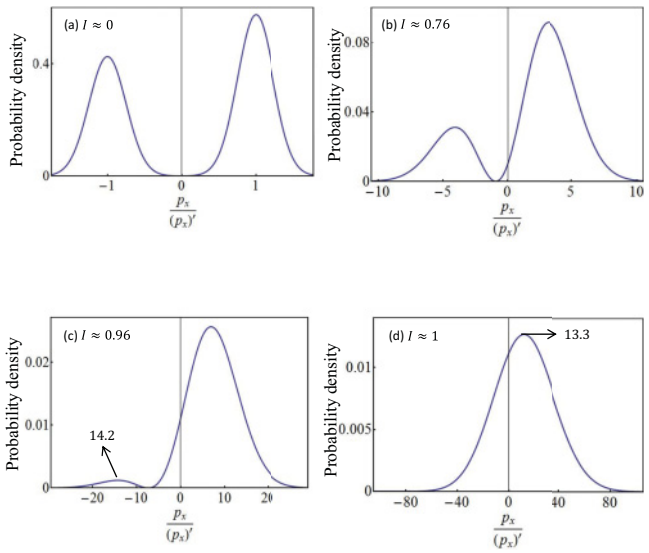

FIG. 3. (Color online) The momentum distribution $|\Phi_{\text{post}}(p_x,\tau)|^2$ [Eq. (29)] is plotted for four values of the inner product (I), depending on the suitable choices of the parameters. (a, d) Strong and weak measurement situations; (b, c) semiweak measurement situations. The weak value is $(\sigma_x)_w = 13.3$ for $\theta = 171^\circ$.

limit. Note, however, that the maximum no longer appears at the eigenvalues or at the usual weak value, Eq. (7), but at the semiweak values, that is, the maximal values of the distribution obtained from Eq. (29). In Fig. 3(c), for example, the left peak is shifted to -14.2 while the weak value is $(\sigma_x)_w = 13.3$ [shown in Fig. 3(d)]. This semiweak value can be chosen at will by tuning the different parameters; approximate analytical expressions may be obtained by expanding $|\Phi_{\text{post}}(p_x,\tau)|^2$ in terms of the relevant small parameters (τ, b, ...or a combination thereof).

3. *Exact weak values*

A different feature of the exact formalism developed above concerns the existence of a meter distribution peaked at eccentric values in the usual weak regime (as far as the weakness of the coupling and the meter states are concerned) but for which the usual AAV formalism does not yield any result. For example, when the initial and postselected states are orthogonal the usual weak value given by Eq. (7) is undefined. This undefiniteness stems from partially expanding the exponential after the postselection [see Eq. (5)]. An exact treatment does not have this problem. Figure 4 shows the exact meter momentum distribution for orthogonal pre- and postselected states, for parameters near the $I \approx 1$ limit. In this situation, the postselected meter state in momentum space is given by

$$\Phi_{\text{post}}(p_x,\tau) = \tfrac{1}{2}[\phi_{+x}(p_x,\tau) - \phi_{-x}(p_x,\tau)]. \qquad (36)$$

The analytical form of the momentum distribution near the $I \approx 1$ limit is readily obtained (up to a constant factor) from the Fourier transform of Eq. (33) as

$$|\Phi_{\text{post}}(p_x,\tau)|^2 \propto p_x^2 \exp\left(-\frac{2p_x^2\delta^2}{\hbar^2}\right). \qquad (37)$$

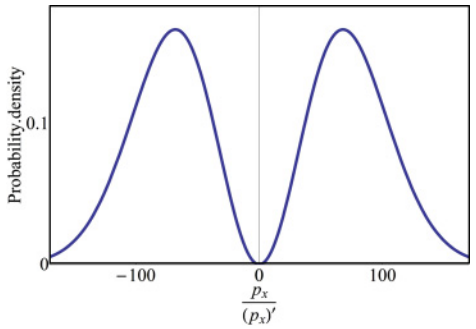

FIG. 4. (Color online) The momentum distribution $|\Phi_{\text{post}}(p_x,\tau)|^2$ [Eq. (36)] is plotted for the case where $I \approx 1$ but the pre- and postselected states are orthogonal—a situation in which the standard weak value is undefined.

This distribution has two peaks at $p_x = \pm\hbar/\sqrt{2}\delta$ as illustrated in Fig. 4. The type of feature illustrated in Fig. 4 was first obtained theoretically in an approximate form (by neglecting the evolution of the pointer inside the SG) by Duck *et al.* [2] and, more recently, revisited in some of the works [20–23] going beyond the standard WM (e.g., in Ref. [21] a formula for orthogonal pre- and postselected states is obtained by considering the interaction up to second order). Experimentally the feature was observed quite early [8]. In a more recent work [25], the electric field analog of Eq. (37) was derived in the framework of a phase-amplification technique using classical wave optics. Note that the exact weak value is perfectly finite, whereas from the definition given by Eq. (7), one might be tempted to conclude [incorrectly, as this would violate the conditions given by Eq. (8), under which the AAV approximation holds] that the weak value can be arbitrarily large as the pre- and postselected states become orthogonal.

Another instance in which the "exact" weak value differs from the one defined in the asymptotic treatment appears when the oscillating terms of the exact solutions [Eq. (30)] play a role. This happens when the wavelength of these terms becomes comparable to the width of the momentum distribution. The first example is shown in Fig. 5, where the pre- and postselected states are identical. Then, according to its definition, (7), the weak value should simply be given by the average of the weakly measured observable in the initial state. It is shown in Fig. 5 that this rule is spoiled by the oscillating terms, which create a multiple peak structure with eccentric maxima. By tuning the parameters entering the exact wave function, the wavelength of the oscillating terms can be reduced, yielding a momentum distribution with multiple peaks, as shown in Fig. 6. The origin of the multiple peaks is the interference between the two meter states emerging from the second SG setup along two opposite directions carrying the opposite phases. These phases (in momentum space) arise because of the separation of the two wave packets in configuration space due to the spin-nonhomogeneous magnetic field interaction occurring along opposite directions. This shows the necessity of the solution of the Schrödinger equation using the full Hamiltonian instead of taking only the interaction Hamiltonian or keeping only a few terms of the asymptotic expansion of the interaction coupling.

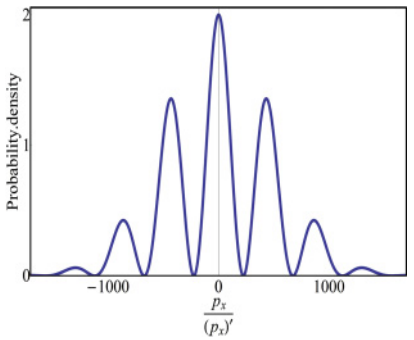

FIG. 5. (Color online) The momentum distribution $|\Phi_{\text{post}}(p_x,\tau)|^2$ [Eq. (29)] is plotted for the case where the pre- and postselected states are identical. Values of relevant parameters: $b = 0.001$ G/cm, $\tau = 1.4 \times 10^{-2}$ s, and $\delta = 5 \times 10^{-2}$ cm.

Note here that the average momentum, which has been the main interest in several studies [20–23], is not necessarily relevant when there are multiple peaks in the momentum distribution.

B. Application: Distinguishing between "identical" density matrices

As an illustration of the practical usefulness of the exact scheme for weak values reported in this work, we give here an application to a quantum information task, namely, the possibility of distinguishing between "identical" density matrices. Consider the following situation: Alice prepares neutral spin-1/2 particles in some state, either ρ_x or ρ_z, and sends them to Bob, whose goal is to guess the state. According to elementary quantum mechanics the spin density matrices

$$\rho_x \equiv \tfrac{1}{2}|\uparrow_x\rangle\langle\uparrow_x| + \tfrac{1}{2}|\downarrow_x\rangle\langle\downarrow_x| \tag{38}$$

$$\rho_z \equiv \tfrac{1}{2}|\uparrow_z\rangle\langle\uparrow_z| + \tfrac{1}{2}|\downarrow_z\rangle\langle\downarrow_z| \tag{39}$$

are identical and thus undistinguishable. We must therefore give an additional condition: We assume that Alice sends successive spins of alternate signs, i.e., Alice sends either $\xi = \{|\uparrow_x\rangle,|\downarrow_x\rangle,|\uparrow_x\rangle,|\downarrow_x\rangle\ldots\}$ or $\zeta = \{|\uparrow_z\rangle,|\downarrow_z\rangle,|\uparrow_z\rangle, |\downarrow_z\rangle\ldots\}$, each of the sets ξ and ζ giving rise to a specific realization of ρ_x or ρ_z, respectively. Bob must guess as quickly as possible, that is, by processing the lowest number of particles, whether Alice is sending ξ or ζ.

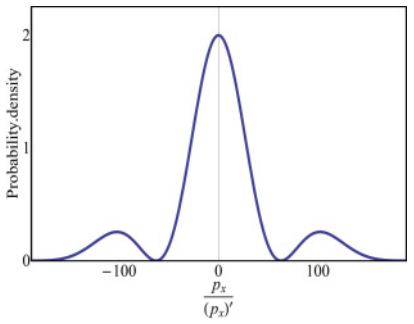

FIG. 6. (Color online) The momentum distribution $|\Phi_{\text{post}}(p_x,\tau)|^2$ [Eq. (29)] is plotted for the case where the pre- and postselected states are identical. Values of relevant parameters: $b = 0.001$ G/cm, $\tau = 1.4 \times 10^{-2}$ s, and $\delta = 10^{-3}$ cm.

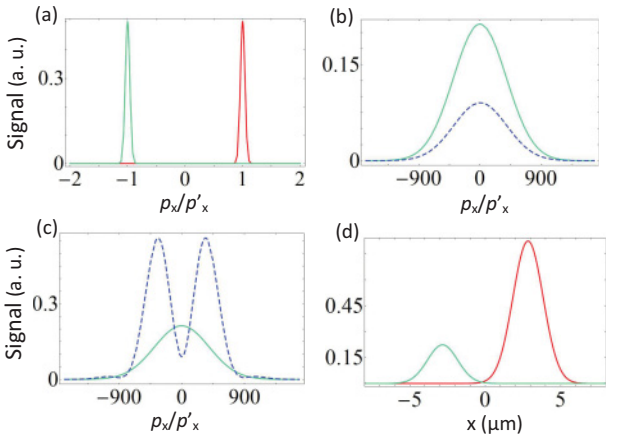

FIG. 7. (Color online) Meter distributions (in arbitrary units) for the task described in Sec. IV 2 for strong (a), standard weak (b), and exact weak (c, d) measurements, with the magnetic field strength fixed in all cases at $b = 0.02$ G/cm and $\tau = 0.07$ s. (a) $\widehat{\sigma}_x$ is measured strongly ($\delta = 1$ cm) and the two peaks appear at the corresponding eigenvalues, irrespective of whether ξ or ζ is being sent. (b) The meter distribution corresponding to ξ [dashed (blue) curve] and to ζ [solid (green) curve] for a standard WM of $\widehat{\sigma}_x$ (with $\delta = 10^{-4}$ cm) and a postselection along 55°. (c) shows the same situation displayed in (b) but with the exact WM solutions. (d) *Configuration*-space meter distributions corresponding to the exact WM momentum-space distributions shown in (c) with the same postselection angle. When Alice launches ξ the left (green) and right (red) peaks are obtained for $|\downarrow_x\rangle$ and $|\uparrow_x\rangle$, respectively, whereas for ζ, $|\downarrow_z\rangle$ and $|\uparrow_z\rangle$ can both hit the left and right peaks.

With strong measurements, the best Bob can do is to measure either $\widehat{\sigma}_x$ or $\widehat{\sigma}_z$ and examine whether two successive measurements have identical signs. Suppose, for instance, that Bob chooses to measure $\widehat{\sigma}_x$; the pointer displays two sharp peaks, one positive and one negative [see Fig. 7(a)]. Then if ξ is sent, the sign of successive outcomes will alternate, whereas if ζ is sent, each outcome is equiprobable. So Bob's strategy will be to observe whether the consecutive measurements have alternating outcomes, in which case he will conclude it is likely that Alice is sending ξ. Indeed, denoting by k the number of particles that have already been seen to be displaying an alternate series, the probability of continuing with this series for the $(k+1)$th particle if ζ has been sent becomes 2^{-k} and decreases rapidly with k.

With standard WMs the problem for Bob is that he ignores the preselected state: he must guess whether Alice is sending ξ or ζ by obtaining meter distributions that are very broad in momentum space, irrespective of the WM and postselection Bob chooses. Typically all the meter distributions have almost-identical profiles but different heights, which is how ξ and ζ can be distinguished [see Fig. 7(b)]. So despite the fact that the meter distributions will indeed be different, in practice, Bob will need a great number of particles in order to discriminate ξ from ζ.

However, by following the exact treatment in the nonideal case, Bob can set (by changing the SG magnetic field strength and passage time) the interference between the meter states in momentum space so that the detection of ξ and ζ result in totally different probability distributions.

Moreover, by weakening the coupling constant, Bob can still keep markedly different profiles in *momentum* space [see Fig. 7(c)]) while obtaining nonoverlapping profiles for the meter in *configuration* space. The advantage is obvious: one has exactly the same information as the one obtained with strong measurements [but in configuration space; see Fig. 7(d)], and in addition, as more particles are detected the detection curve in momentum space unambiguously reveals whether ξ or ζ is being sent. It is crucial to note that the two distinctly positioned peaks visible in configuration space are a feature of the exact solutions: in the standard WM formalism the configuration-space wave functions are identical up to some global factor. In practice [26], each odd-numbered result is registered separately from the even-numbered events, and this is done for each of the two postselected states. The procedure can be stopped when enough events are registered so that the curves can be discriminated by employing standard statistical tests minimizing the distance between the expected curve and the obtained outcome [26].

V. SUMMARY AND CONCLUSIONS

In this work we have derived the exact behavior of a measurement apparatus for arbitrary nonideal measurements. This was done in the analytically tractable case of a spin measurement in SG setups, for which the exact time-dependent wave functions can be obtained. This has allowed us to investigate the validity of the usual AAV WM formalism, both in the intermediate regime, far from the usual WM limit, and in the WM limit when the specific features of the system-meter interaction are explicitly accounted for. In doing so, we have been led to introduce "semiweak" and "exact weak" values that describe the meter distribution and the associated eccentric values in these circumstances (including, but not limited to, the case of orthogonal pre- and postselected states, for which the usual weak value is undefined).

We have also seen through our exact approach that including the full Hamiltonian (rather than restricting the treatment to the interaction Hamiltonian) may have crucial consequences for the behavior of the eccentric values. In this sense, an exact approach brings features in addition to those that can be retrieved by the approaches in other recent work [20–23] dealing with extending the original WM approach: It is valid irrespective of the interaction strength and it yields fine details due to the specificities of the interaction. On the other hand, the practical applicability of an exact approach hinges on the ability to solve (analytically or numerically) the full Schrödinger equation, a task that can become difficult for an arbitrary system. In all cases, going beyond the usual WM formalism as well as the relevance of performing exact calculations for a given experimental situation should be helpful in analyzing experimental results obtained in nonideal measurements.

[1] Y. Aharonov, D. Z. Albert, and L. Vaidman, Phys. Rev. Lett. **60**, 1351 (1988).

[2] I. M. Duck, P. M. Stevenson, and E. C. G. Sudarshan, Phys. Rev. D **40**, 2112 (1989).

[3] Y. Aharonov and L. Vaidman, J. Phys. A **24**, 2315 (1991).

[4] G. Mitchison, R. Jozsa, and S. Popescu, Phys. Rev. A **76**, 062105 (2007).

[5] J. Tollaksen, J. Phys. A**40**, 9033 (2007).

[6] R. Jozsa, Phys. Rev. A **76**, 044103 (2007).

[7] N. Brunner and C. Simon, Phys. Rev. Lett. **105**, 010405 (2010).

[8] N. W. M. Ritchie, J. G. Story, and R. G. Hulet, Phys. Rev. Lett. **66**, 1107 (1991).

[9] Q. Wang, F. W. Sun, Y. S. Zhang, J. Li, Y. F. Huang, and G. C. Guo, Phys. Rev. A **73**, 023814 (2006).

[10] G. J. Pryde, J. L. OBrien, A. G. White, T. C. Ralph, and H. M. Wiseman, Phys. Rev. Lett. **94**, 220405 (2008).

[11] O. Hosten and P. Kwiat, Science **319**, 787 (2008).

[12] K. Yokota, T. Yamamoto, M. Koashi, and N. Imoto, New J. Phys. **11**, 033011 (2009).

[13] D. J. Starling, P. B. Dixon, A. N. Jordan, and J. C. Howell, Phys. Rev. A **80**, 041803(R) (2009).

[14] J. S. Lundeen and A. M. Steinberg, Phys. Rev. Lett. **102**, 020404 (2009).

[15] A. P. Lund and H. M. Wiseman, New J. Phys. **12**, 093011 (2010).

[16] O. Zilberberg, A. Romito, and Y. Gefen, Phys. Rev. Lett. **106**, 080405 (2011).

[17] L. Vaidman, Found. Phys. **26**, 895 (1996).

[18] Y. Aharonov, A. Botero, S. Popescu, B. Reznik, and J. Tollaksen, Phys. Lett. A **301**, 130 (2002).

[19] S. Kocsis, B. Braverman, S. Ravets, M. J. Stevens, R. P. Mirin, L. K. Shalm, and A. M. Steinberg, Science **332**, 117 (2011).

[20] T. Geszti, Phys. Rev. A **81**, 044102 (2010).

[21] S. Wu and Y. Li, Phys. Rev. A **83**, 052106 (2011).

[22] K. Nakamura, A. Nishizawa, and M. K. Fujimoto, e-print arXiv:1108.2114 (2011).

[23] X. Zhu, Y. Zhang, S. Pang, C. Qiao, Q. Liu, and S. Wu, Phys. Rev. A **84**, 052111 (2011).

[24] D. Home, A. K. Pan, Md. M. Ali and A. S. Majumdar, J. Phys. A **40**, 13975 (2007); D. Home and A. K. Pan, *ibid*. **42**, 165302 (2009).

[25] D. J. Starling, P. B. Dixon, N. S. Williams, A. N. Jordan, and J. C. Howell, Phys. Rev. A **82**, 011802(R) (2010).

[26] A. K. Pan and A. Matzkin, Laser Phys. (in press, 2012).